

# **Carbon fiber as primary target at the hypernuclear experiment of $\overline{\text{PANDA}}$**

von

**Birte Sauer**

Bachelorarbeit in Physik  
vorgelegt dem Fachbereich Physik, Mathematik und Informatik (FB 08)  
der Johannes Gutenberg-Universität Mainz  
am 13. Februar 2018

1. Gutachter: Prof. Dr. Josef Pochodzalla
2. Gutachter: Prof. Dr. Eva-Maria Kabuß



Ich versichere, dass ich die Arbeit selbstständig verfasst und keine anderen als die angegebenen Quellen und Hilfsmittel benutzt sowie Zitate kenntlich gemacht habe.

Mainz, den 13.02.2018

Birte Sauer  
SPECF  
Helmholtz-Institut Mainz  
Staudingerweg 18  
Johannes Gutenberg-Universität D-55099 Mainz  
bisauer@students.uni-mainz.de



# Abstract

Diese Bachelorarbeit wurde im Rahmen des Hyperkernexperiments an  $\bar{P}$ ANDA verfasst und beschäftigt sich mit der Eignung von Kohlenstofffasern als Primärtarget in Streuversuchen. Insbesondere wird dabei auf das Klebeverhalten der Faser auf Aluminiumrahmen und das Verhalten einzelner Fasern unter thermischer Belastung durch elektrischen Strom eingegangen. Letzteres dient der Simulation der thermischen Bedingungen im Streuexperiment.

Die Suche nach einem geeigneten Kleber gestaltet sich schwierig da dieser vakuumtauglich und elektrisch leitend sein muss ebenso wie er das Experiment nicht durch die Aktivierung von Partikeln wie beispielsweise Silberionen stören darf. Keiner der getesteten Kleber konnte komplett überzeugen, jedoch ist ein Trend in Richtung Epoxid-Kleber oder Leitlack erkennbar.

In den Experimenten konnten die getesteten Fasern durch Langlebigkeit überzeugen. Sowohl in Luft als auch in Vakuum überleben die Fasern erheblich größere thermische Leistungen als von  $\bar{P}$ ANDA erwartet werden. Die größte von  $\bar{P}$ ANDA erwartete Leistung halten die Fasern lange genug aus um darauf reagieren zu können und das Target weiter aus dem Strahl heraus fahren zu können. In Langzeittests bei kleinen Spannungen zeigen sich die Fasern sehr beständig, allerdings wurden hier auch Schwachstellen im Versuchsaufbau in Form von Kontaktproblemen deutlich.

Wenn die Faser auch in Strahltests überzeugen kann, ist sie eine günstigere und einfacher herzustellende Alternative als die bisher in Betracht gezogenen Diamantplättchen.



# Contents

<b>1. Introduction</b>	<b>1</b>
1.1. The hypernuclear experiment at $\overline{\text{PANDA}}$ . . . . .	1
1.2. Primary target . . . . .	4
1.3. Carbon fibers . . . . .	7
<b>2. Construction of single filament targets for the hypernuclear <math>\overline{\text{PANDA}}</math> experiment</b>	<b>8</b>
2.1. Obtaining an individual carbon filament from a thread . . . . .	8
2.2. The glueing of fiber and frame . . . . .	9
<b>3. Thermal behavior of carbon fibers</b>	<b>13</b>
3.1. Experimental setup . . . . .	13
3.2. Verification of the expected electrical resistance value . . . . .	15
3.3. Thermal influences in vacuum and air . . . . .	18
3.4. Simulation of thermal stress expected from $\overline{\text{PANDA}}$ . . . . .	23
<b>4. Summary and outlook</b>	<b>28</b>
<b>A. Appendix</b>	<b>30</b>
A.1. Production of carbon filaments via PAN . . . . .	30
A.2. Further figures and tables . . . . .	31
<b>B. Bibliography</b>	<b>35</b>
<b>C. List of Figures</b>	<b>37</b>
<b>D. List of Tables</b>	<b>38</b>



# 1. Introduction

The hypernuclear experiment at  $\bar{\text{P}}\text{ANDA}$ <sup>1</sup> produces  $\Xi^-$  via annihilation of antiprotons on a internal nuclear target. Thin targets are required for this inside the HESR<sup>2</sup> of FAIR<sup>3</sup>. Carbon fiber filaments seem to be a reliable option.

Besides a small overview of this experiment the first chapter focuses on the setup of the primary target, previous studies and calculations of materials for the primary target. Afterwards a procedure to separate single filaments from a thread is described. Various glues are compared in their suitability to fix the fragile filament to a holding frame. The final experimental chapter presents simulations of the thermal conditions expected at  $\bar{\text{P}}\text{ANDA}$  via induction of an electric current. High power and long-term experiments are performed. Finally, a conclusion and an outlook is presented.

## 1.1. The hypernuclear experiment at $\bar{\text{P}}\text{ANDA}$

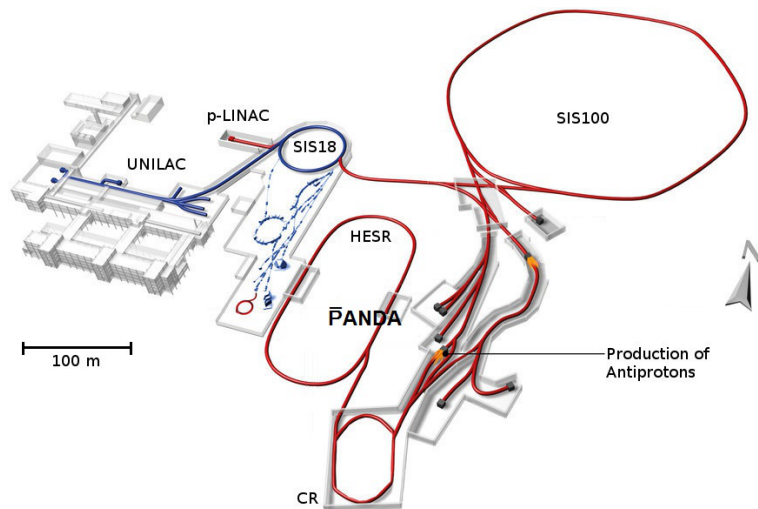


Figure 1.1.: The conceptual setup of FAIR and its integration at GSI ([Col05])

In Darmstadt the existing GSI Helmholtzzentrum für Schwerionenforschung is expanded by FAIR, a new research facility which is currently under construction. The

<sup>1</sup>Anti-Proton Annihilation at Darmstadt

<sup>2</sup>High Energy Storage Ring

<sup>3</sup>Facility for Antiproton and Ion Research

## 1. Introduction

$\bar{\text{PANDA}}$  experiment at FAIR will focus on the interaction of antiprotons with fixed targets in a momentum range of 1.5 - 15 GeV/c. The antiprotons are stored at the high energy storage ring HESR with up to  $10^{10}$  antiprotons per cycle. Since instant refilling is not possible the number of antiprotons decreases, due to reactions in the target and scattering. This limits the maximum length of the cycle.

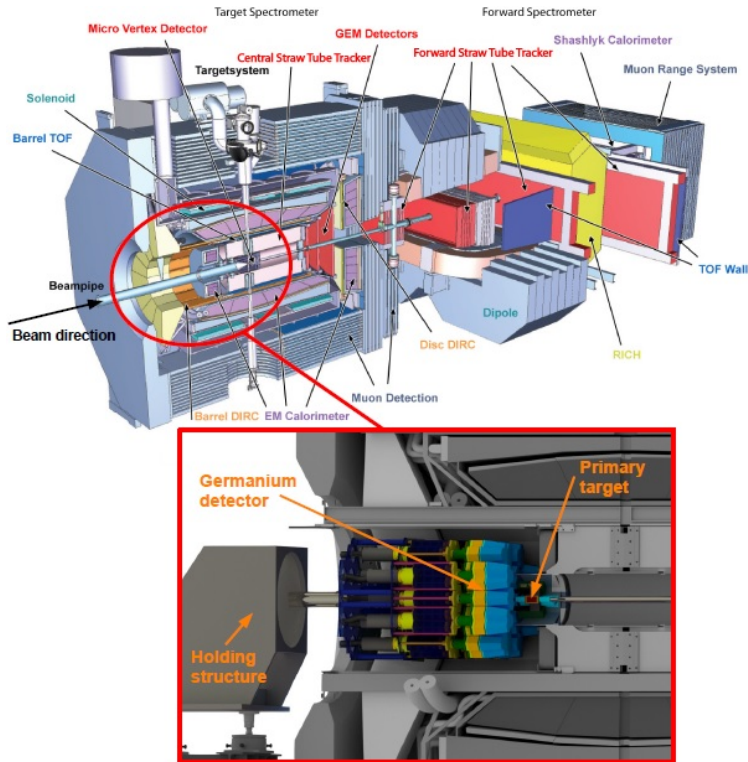


Figure 1.2.: The complete overview of standard  $\bar{\text{PANDA}}$  [Col05]. The hypernuclear experiment will be integrated in the marked area and is displayed in the smaller image.

## 1. Introduction

The  $\bar{\text{P}}\text{ANDA}$  experiment includes several fixed target experiments, one of which is the hypernuclear experiment. It consists of a staged target system divided into primary and secondary target as well as a dedicated germanium detector cluster (figure 1.2). One of its purposes is the study of double  $\Lambda$  hypernuclei by performing high precision  $\gamma$  spectroscopy. A hypernucleus is made up of neutrons and protons alongside at least one hyperon, a baryon consisting of a minimum of one strange quark. The  $\Lambda$  hyperon is comprised of a strange, up and down quark resulting in a strangeness of  $S = -1$ .

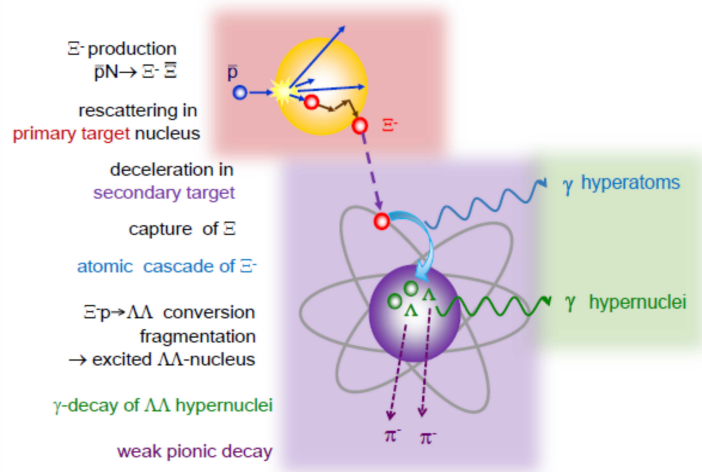
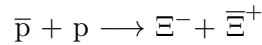
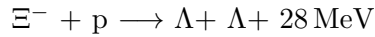


Figure 1.3.: Representation of hypernuclei production

The production of hypernuclei is achieved in two steps. The antiprotons with a momentum of  $3 \text{ GeV}/c$  collide with nuclei inside the primary target producing  $\Xi$  particles.



These particles leave the primary target and are decelerated and captured within the secondary target. After an atomic cascade, double  $\Lambda$  nuclei are produced inside the absorber nuclei of the secondary target.



Due to the excessive energy, these hypernuclei occupy highly excited states and a fragmentation takes place in which the two  $\Lambda$  can remain together in one of the fragments. This double  $\Lambda$  hypernucleus then deexcites by emitting gammas which are measured in the germanium detector array. When the hypernucleus decays pions are emitted which are tracked in the silicon detector layers of the secondary target.

## 1. Introduction

### 1.2. Primary target

The primary target has to be a thin filament so that  $\Xi^-$  can leave it. Also, the production rate and the loss of antiprotons are influenced by the thickness of the target.

As seen in figure 1.4, the target is placed on a frame mounted onto piezo motors. These motors allow the precise positioning within the beam pipe since the target will be placed in the halo of the antiproton beam under normal operation conditions and has to be repositioned once the intensity of the beam decreases.

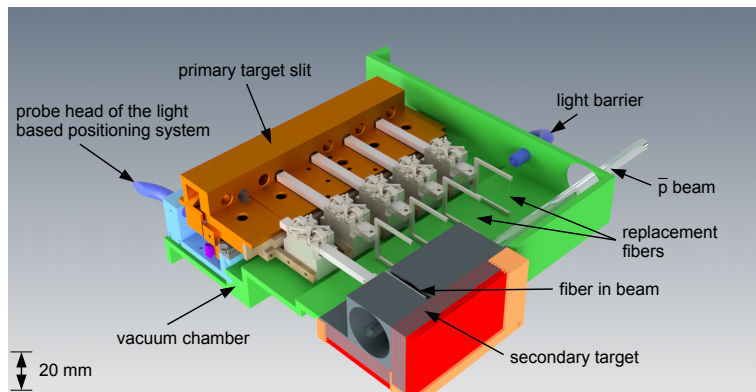


Figure 1.4.: CAD design of the primary target setup. The targets are mounted on frames connected to piezo motors allowing precise positioning within the beam pipe

The production rate of  $\Xi^-$  in the primary target is crucial to the experiment, yet the momenta of the  $\Xi^-$  must be less than 500 MeV/c in order to stop it in the secondary target. The antiprotons stored within the beam should not be wasted in order to maintain the efficiency of the experiment. This results in a compromise trying to optimize between both requirements which can best be achieved by using light nuclei such as carbon, silicon or titanium. The latter two have been discarded since the rate of lost antiprotons outweighs the production rate of  $\Xi^-$  [Ble18] (compare table 1.5). Carbon offers high production rates of  $\Xi^-$  while keeping the loss of antiprotons lower than the other materials. It is therefore the most ideal target material so far.

## 1. Introduction

Target-material	$\Xi^-$ production probability	$\Xi^-$ stopping probability	Luminosity loss factor	FoM
$^{12}\text{C}$	$(2.22 \pm 0.02) \cdot 10^{-5}$	$(3.24 \pm 0.04) \cdot 10^{-3}$	0.539	$(3.87 \pm 0.06) \cdot 10^{-8}$
$^{28}\text{Si}$	$(2.42 \pm 0.04) \cdot 10^{-5}$	$(3.41 \pm 0.07) \cdot 10^{-3}$	0.339	$(2.80 \pm 0.08) \cdot 10^{-8}$
$^{48}\text{Ti}$	$(2.48 \pm 0.04) \cdot 10^{-5}$	$(3.79 \pm 0.07) \cdot 10^{-3}$	0.245	$(2.31 \pm 0.05) \cdot 10^{-8}$

Figure 1.5.: Extract from [So16] displaying the expected production and stopping probabilities for  $\Xi^-$  in 3 possible materials as well as their overall luminosity loss factor and a figure of merit (FoM) obtained by multiplying the preceding values.

Target material	P @ R = $4 \cdot 10^6$ inter./s	P @ R = $4 \cdot 10^7$ inter./s	P @ Max. overlap
Diamond	0.056 mW	0.56 mW	11.3 mW
DIALEAD	0.056 mW	0.56 mW	7.1 mW
Sigrafil	0.056 mW	0.56 mW	5.8 mW
Silicon	0.080 mW	0.80 mW	7.1 mW
Titanium	0.091 mW	0.91 mW	12.4 mW

Figure 1.6.: Extract from [Ble18] displaying the obtained data from a heat simulation for 15 scenarios

In order to further investigate the thermal behavior of all possible target materials, a heat simulation was conducted [Ble18]. The data obtained in this simulation (figure 1.6) will be the reference for the experimental studies in chapter 3. The obtained temperature is displayed in 1.7. All targets remain well beneath their critical temperatures above their melting points. The range above the graphitization temperature for diamond is marked differently but is also not reached.

## 1. Introduction

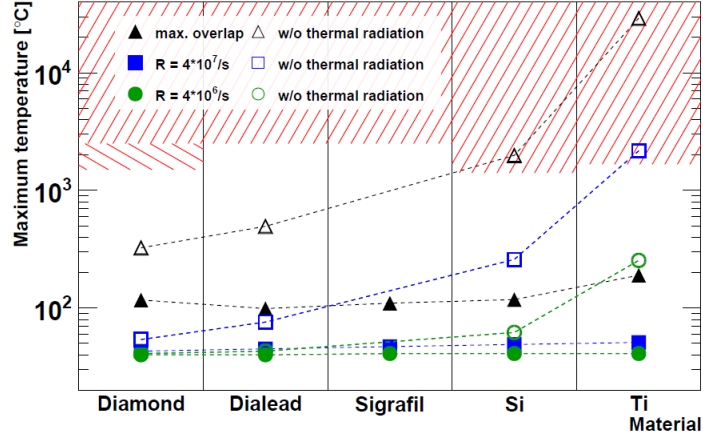


Figure 1.7.: Extract from [Ble18] displaying the expected maximum temperature in the discussed scenarios both with and without thermal radiation. The simulation of Sigrafil has only been performed with thermal radiation. In the updated version with thermal radiation no material reaches temperatures above its melting point (red marked areas).

Two implementations of carbon have been considered for the target: CVD diamond cut into a thin filament and carbon fibers. The former has already been tested [Roj16] while the latter still has to be investigated. A comparison between two types of carbon fibers and the CVD diamond is displayed in table 1.1. The data was collected from [Roj16],[Sig] and [Che].

	Diamond	Dialead	Sigrafil
tensile modulus [GPa]	1050 - 1210	935	270
tensile strength [GPa]	0.5 - 1.4*	3.7	5.0
thermal conductivity [W/mK]	1800 - 2500	800	<100*
electrical resistivity [ $\mu\Omega\text{m}$ ]	>10 <sup>20</sup> *	8	14
density [g/cm <sup>3</sup> ]	3.52	2.2	1.81

Table 1.1.: Comparison between the 3 possible carbon based materials. No value for the properties marked with \* was available, however the value for Sigrafil could be approximated through [Che] while the diamond data is obtained from [diab]

The test with a diamond filament as target material in an electron beam revealed brown imprints on the both the front and back side of the surface of the target. A surface analysis through Raman spectroscopy showed that the diamond was destroyed leaving graphite in its place [Ble18].

If the initial structure of the primary target is destroyed during the experiment, a

## 1. Introduction

carbon fiber based target might be constructed more easily while contributing similar production rates of  $\Xi^-$  and being more cost efficient.

### 1.3. Carbon fibers

The carbon fiber thread always consists of several thousand filaments. Due to its relative large strength compared to its thickness, the thread is used in fiber-reinforced composites. It can be produced starting from PAN<sup>4</sup> or pitch. Although both types of fibers share a structure comparable to graphite, the resulting filaments differ in their physical properties due to a different substructure. While pitch based fibers consist of individual layers, the PAN based fiber is made up of a tube like consistant cluster. Both types of fibers have been considered for the experiment namely "SIGRAFIL® C T24-5.0/270-E100" distributed by SGL Group as PAN based fiber [Sig] and "Dialead K13D2U" distributed by Mitsubishi Rayon Co. [Diaa] based on pitch. In the following, the fibers will be addressed as Sigrafil and Dialead respectively. Sigrafil's mechanical stability is its crucial property while Dialead is chosen due to its high thermal conductivity.

In preparation for chapter 2.3 the thermal dependency of the resistance of graphite is studied. This relation can be applied on both fibers due to their similar structure and thereby compensates the lack of data concerning the individual filaments.

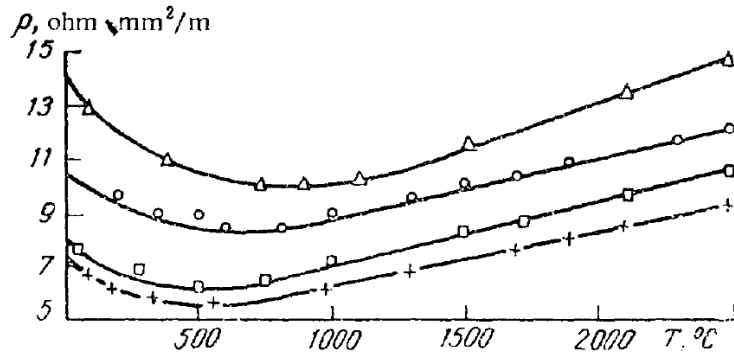


Figure 1.8.: Extract from [LFM62] displaying the thermal behavior of graphite in respect to its specific resistance. Its overall behavior is independent of the chosen material. Within the range up to 500 °C the specific resistance decreases while it increases afterwards.

As shown in 1.8, an extract from [LFM62], the relative resistance first decreases with increasing temperature. At around 500 °C the minimum is reached. With further increase in temperature the relative resistance also rises. This can be used to determine an approximation of the temperature encountered during the measurements in chapter 3.

<sup>4</sup>PolyAcryloNitrile

## 2. Construction of single filament targets for the hypernuclear $\overline{\text{PANDA}}$ experiment

This chapter treats the handling of the fiber as well as tests concerning the construction of a single filament based primary target at the hypernuclear  $\overline{\text{PANDA}}$  experiment. First it is discussed how one single filament can be separated from the thread, followed by observations during the adhesive bounding onto the frame.

### 2.1. Obtaining an individual carbon filament from a thread

The commercial purpose of carbon fibers is to build fiber-reinforced composites. It can not be purchased as single filaments but is sold in continuous carbon fiber tows with up to 24.000 single filaments. A procedure to unravel the thread manually has to be found.

For the experiment, the two carbon fibers mentioned earlier are used. The stability of the single filament was uncertain before the fibers could be scrutinized since the data sheets only present data concerning the whole thread instead of the single filament. The pitch based fiber Dialead is shipped wound onto a role. Uncoiling the role of Dialed it is noted that the fiber appears brittle. The thread breaks upon the application of slight mechanical force. To check whether this property might have been caused during shipment, the thread is also examined after unraveling the fiber for approximately one meter. However its frail characteristic remained. Due to its brittle structure, Dialead is discarded.

The test sample of Sigrafil acquired from SGL Carbon group contained a one meter long thread stored within a transparent sheet. The thread already frays. It reacts similarly as hair to minor electric charges loaded in plastic.

Concerning its thin diameter of  $7\ \mu\text{m}$  per filament, separating the thread turns out difficult since one can barely locate the filament. Using a desk magnifying glass with an incorporated light source improves the visibility of the fiber. Trying to separate the fiber using a pair of tweezers snapped it, therefore the separation of the thread is performed without the use of tools. By tapping onto the frayed fiber the separation can be pursued. Once it moves apart far enough, a smaller fraction of the fiber can be detached at the required length. Sometimes it is not entirely possible to separate the last few filaments through mechanical forces.

## 2. Construction of single filament targets for the hypernuclear $\bar{P}$ ANDA experiment



Figure 2.1.: Sigrafil thread, its end is already frayed

The final determination whether one single fiber has been selected is hardly possible using an optical examination, but measuring the electrical resistance of the test fiber allows to distinguish between a single or multiple filament in parallel. However, in the next section the number of fibers is insignificant and the detailed description of this measurement will be delayed until chapter 3.

### 2.2. The glueing of fiber and frame

In the  $\bar{P}$ ANDA experiment, the primary target has to be thin in order to allow the  $\Xi^-$  hyperons to leave it. Since the filament has to be moveable within the beam pipe, it needs to be secured to a positioning device.

The CAD drawing of a frame bridging fiber and piezo motor is presented in the appendix A.2 as proposed in [Ble18]. This frame consists of a 1 mm thick metal C-form extended into a thin plate which features a screw hole allowing to mount it. Two materials for the frame are available. One is made from aluminium while the material of the other frame is titan. The former is produced in a larger quantity therefore it has been chosen as test frame. The results of the glueing tests should also be applicable to the other frame.

## 2. Construction of single filament targets for the hypernuclear $\bar{P}$ ANDA experiment

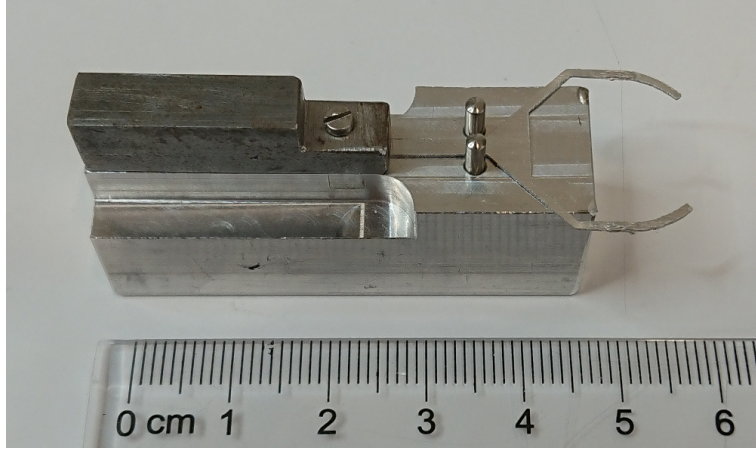


Figure 2.2.: Metal block with frame made from aluminium, the C-form is covered with conductive silver varnish. The fiber glued onto it is barely visible.

To improve the handling of the frame, an additional tool has been designed to allow a raised view onto the holder enabling undisturbed operations on both top and bottom. It consists of a broad base onto which the frame is secured with another thinner metal block screwed on top of it. Figure 2.2 shows the tool with a frame mounted in between. The fiber is supposed to be placed between the arms of the frame. Figure 2.3 shows a filament glued onto the frame with conductive silver varnish.

In order to fix the filament onto the frame, an appropriate glue had to be found. The durability and suitability of four different types of glues were tested. On one hand, the glues should be simple in their handling, vacuum capable and radiation resistant as well as electroconductive. On the other hand, they should not produce long-lived isotopes through activation such as silver ions or stress the fiber too much while drying, e.g. through heat development.

Uhu multi-purpose adhesive [Uhu] is chosen as reference. It is based on polyvinyl acetat. This glue is not fit for vacuum and hence will highly outgas in the ultra high vacuum of the beam pipe within  $\bar{P}$ ANDA. Nevertheless, it is used as a first step to study both frame and fiber in contact with an adhesive and serves as reference for the other glues.

The first test glue is Pattex Ultra Gel [Pat] which is based on ethyl canoacrylate. This superglue is easily obtainable as well as cheap and well manageable, however it generates heat while drying.

## 2. Construction of single filament targets for the hypernuclear $\bar{P}$ ANDA experiment

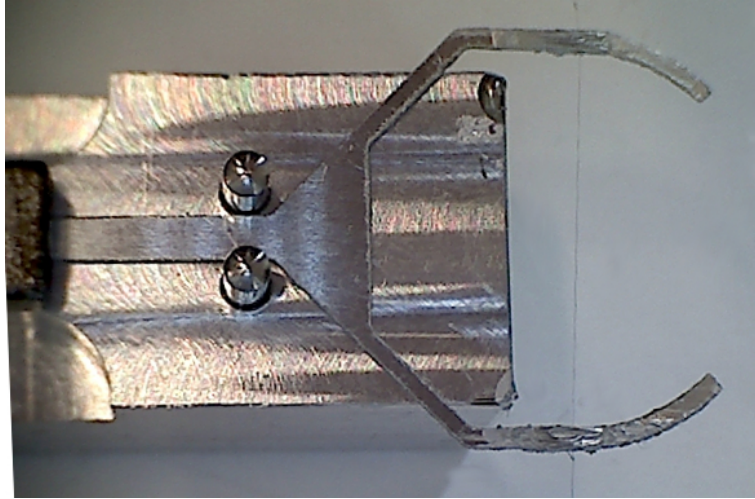


Figure 2.3.: Aluminium frame with a filament glued onto it using conductive silver varnish

Next, Arctic MX-2 Thermal Compound [Arca] and Arctic Silver<sup>TM</sup> Thermal Adhesive [Arcb] were tested. They are specialized in heat transmission. Before applying the glue to the frame, its two components have to be mixed together in a 1:1 ratio. However, the glue has a small proportion of silver ions, therefore an alternative that does not have ions is considered. As it will barely differ in their mechanical behavior a test of it has been renounced.

The final test treated conductive silver varnish, type RS 186-3593 [Tar]. Since this glue consists of silver and is therefore prone to produce silver ions, an alternative has been considered, namely a similar varnish based on carbon. This glue has not been available while testing therefore the silver varnish was tested instead.

All adhesives can be treated equally, however they differ greatly in their application and drying time. It is the best to rub the glue onto the frame and leaving it to become dry to the touch before adding the fiber because the glue would not smear the filament as much. The sharp edges of the frame cause the filament to break easily, it is therefore necessary to be careful not to stress the fiber over the edges. Its application is performed by straining the fiber and pressing it on top of the frame. Choosing a filament with a length of about three times the distance between the arms of the frame is advised so that the endpieces of the fiber can be gripped more easily.

### multi-purpose adhesive

It dries quickly within few minutes and holds the filament in position. Slightly blowing against the filament resulted in its slight swing. This indicates that the fiber began to sag during the drying process. This is not ideal for its usage in  $\bar{P}$ ANDA since the localization of the target is easier if the fiber is stiff. The frame showed no affects by the glue.

## 2. Construction of single filament targets for the hypernuclear $\bar{P}$ ANDA experiment

superglue

The drying time had been decreased, the heat development caused the fiber to contract due to its negative coefficient of thermal expansion. Therefore the probability that the fiber ruptures is not negligible. Due to the contraction, the fiber is firmly secured onto the frame, but the frame showed white discolorations where the glue is applied indicating a form of oxidation. Both the oxidation and the rupture of the fiber are undesirable for  $\bar{P}$ ANDA and it is unlikely that the glue persists in vacuum therefore this glue is discarded.

thermal compound

Its prolonged drying time and insufficient hold on the fiber caused the fiber to slip covering it in paste or losing it completely. The frame is unaffected.

two component glue based on epoxy resin (Arctic Silver<sup>TM</sup> Thermal Adhesive)

This glue is considered the best option so far. Its drying time and heat emission are both located within reasonable scales. A sufficient dryness is obtained after around 2 minutes. No rupture or dislocation of the fiber could be observed. Also, using a heat gun to test its durability under high temperatures and air flow yielded no impairment in the holding ability of the glue.

conductive silver varnish (RS 186-3593)

Similar to the two component glue, this glue dries quickly and does not damage the fiber through heat emission. Also, the frame is unaffected by it. The glue was recently considered for the experiment, therefore further testing is not yet performed. It seems to be an alternative to the two component glue and since the silver is not ionized, it should be fine in vacuum. The glue can be cleaned off using acetone, allowing the reuse of the frame if the fiber is destroyed.

This experiment could not single out the perfect glue for connecting frame and fiber, however a trend towards a two component glue based on epoxy resin without silver ions or conductive carbon varnish is established. Also, ordinary glues can be discarded as well as any adhesive that includes ions whose activation might interfere with the  $\bar{P}$ ANDA experiment.

## 3. Thermal behavior of carbon fibers

In this chapter, the experiments with the fiber are discussed. The setup is presented first, followed by the measurement of the resistance of the fiber and its comparison to the calculated value. Afterwards the heating process of the filament inside the HESR beam is simulated. This is done by applying a constant voltage to it. Measurements with increasing voltage as well as long-term measurements with constant voltage will be shown.

### 3.1. Experimental setup

The experiment studies the durability of the fiber under the expected thermal stress at the hypernuclear  $\bar{\text{P}}\text{ANDA}$  experiment by inducing electrical power.

Since the filament will be in vacuum during the experiment, similar conditions have to be achieved. Therefore the setup will be put inside the vacuum chamber of a Thermo Scientific VACUTherm vacuum oven. It is not used to heat up the fiber but its big vacuum chamber allows easy installation of the setup especially since an electrical feedthrough is already intended. Flooding the chamber with air allows direct comparison without changing the setup displayed in figure 3.1.

Outside the vacuum chamber several constant-voltage generators connected in series supply voltages in the range of 0 V to 210 V to the fiber. A multimeter, type "Benning MM10" [Ben], is included to measure the current passing the fiber. Since the measured currents are in the  $\mu\text{A}$  range the internal resistance of the multimeter can't be neglected<sup>1</sup> and the voltage applied to the fiber has to be measured directly at the vacuum feedthroughs using an "Agilent U1272A" [Agi].

---

<sup>1</sup>voltage drop in the multimeter:  $\leq 4\text{ mV}/\mu\text{A}$  [Ben]

### 3. Thermal behavior of carbon fibers

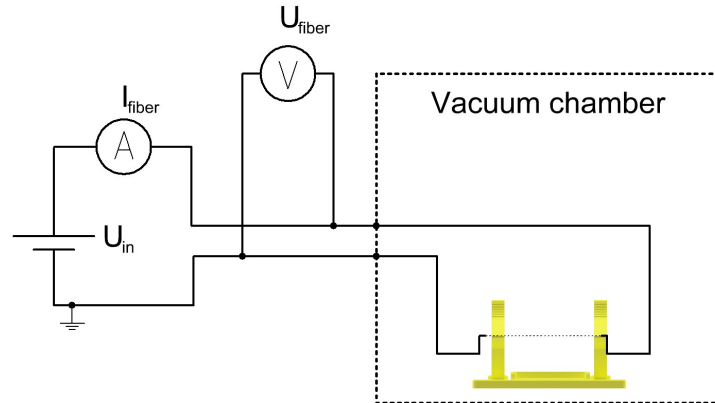


Figure 3.1.: Circuit diagram

The voltage  $U_{in}$  is applied to the circuit. The current ( $I_{fiber}$ ) is measured by a multimeter before passing the fiber within the vacuum chamber. The voltage  $U_{fiber}$  applied to the fiber is measured directly at the vacuum feedthroughs. It differs from the supplied voltage due to the not negligible internal resistance of the first multimeter when measuring in  $\mu A$  range.

The carbon fiber is difficult to handle. To allow the fixing of a single fiber a holding frame is designed and 3D-printed, shown in 3.2. The ABS synthetic material used to print the holder is nonconductive and able to withstand the required vacuum conditions for the test in an environment of a few mbar.

### 3. Thermal behavior of carbon fibers



Figure 3.2.: This picture shows the holding device used throughout the experiments. It consists of a 3D-printed nonconductive frame onto which two copper plates with plugs are applied. The fiber can be pressed onto these plates allowing its inclusion into a circuit.

The model of the frame is composed of two identical pieces each consisting of an upper and a lower part connected via spring. The lower parts can be bolted onto a plate at a fixed distance of 7 cm. The upper part is slightly bent upwards on one end to allow the user to open the holder with one hand. The inclusion of the fiber into the electric circuit is achieved by adding two copper plates with cable plugs to the frame. To protect the fiber from rupture due to the hard synthetic material of the frame, each upper part of the frame is covered with foam rubber.

#### 3.2. Verification of the expected electrical resistance value

The fiber can barely be seen with the naked eye and sometimes few filament groups consisting of 2 to 3 fibers can not be separated through application of mechanical force. It was therefore apparent that the best test to assure the presence of a single filament is to measure its electrical resistance. A single fiber would yield an electrical resistance around the expected  $29.1\text{ k}\Omega$  calculated in equation 3.1 while multiple threads will be measured parallel therefore decreasing the resistance to a fraction of its expected value. A simple multimeter connected to the copper plates when the filament is inside the holding frame suffices to perform this test.

The experiment is first conducted in air and then in vacuum. This order is reasonable since the fiber can only be added into the frame while it is in air, but in one occasion,

### 3. Thermal behavior of carbon fibers

labeled "2", the air siphoning caused the loss of the fiber. This indicates that the fiber was not tightly secured.

According to [Sig], the specific resistance of an individual filament is  $14 \mu\Omega\text{m}$ . Using formula (3.1) this results in a resistance of  $29.103 \text{ k}\Omega$ , which is treated as reference value in this chapter.

$$R = \rho \times \frac{l}{A} \approx 29.1 \text{ k}\Omega \quad (3.1)$$

R: electric resistance,  $\rho$ : specific resistance ( $14 \mu\Omega\text{m}$ ), l: fiber length (7 cm)  
A: cross section area (circular),  $A = \pi \times \frac{d^2}{4}$ , d: diameter of the fiber ( $7 \mu\text{m}$ )

medium	fiber	R [k $\Omega$ ]	$\Delta R_{\text{mm}}$ [k $\Omega$ ]	$A_{29 \text{ k}\Omega}$ [%]	$\Delta_1$ [%]
air	1	27,3	0,1	93,9	–
	2	28,0	0,1	96,3	2,5
	3	29,0	0,2	99,8	6,2
	4	28,8	0,1	98,8	5,2
	5	28,9	0,1	99,4	5,8
vacuum	1	26,9	0,1	92,5	1,5
	3	29,0	0,1	99,5	5,9
	4	28,3	0,1	97,4	3,6
	5	27,7	0,1	95,3	1,5

Table 3.1.: Table displaying resistance R of a single filament with deviation  $\Delta R_{\text{mm}}$  in accordance with [Ben], its relative accordance  $A_{29 \text{ k}\Omega}$  with the calculated value for the resistance and the relative deviation  $\Delta_1$  to fiber 1. Fiber 2 could not be measured in vacuum since it had been lost during the evacuation of the vacuum chamber.

### 3. Thermal behavior of carbon fibers

Table 3.1 shows the measured resistances  $R$  and its relative accordance  $A_{29\text{k}\Omega}$  to the calculated value 3.1 and the relative deviation  $\Delta_1$  to one of the fibers labeled "1" in the table. The latter is determined via

$$\Delta_1 = \left| 1 - \frac{R_{\text{measured}}}{R_{\text{fiber 1}}} \right|$$

while the accordance is determined by

$$A_{29\text{k}\Omega} = \left| \frac{R_{\text{measured}}}{R_{\text{calculated}}} \right|$$

It has to be noted that both the length of the section and the diameter of the fiber are subject to errors hence an estimation concerning the deviation of this value has to be made by gaussian error propagation.

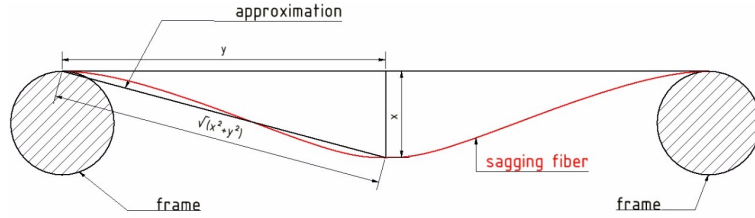


Figure 3.3.: Approximation concerning the deviation in the length of the tested section due to the sagging of the fiber based on Pythagoras' theorem

Through Pythagoras' theorem an approximation of the deviation of the length of the section is obtained, compare equation (3.2) and figure 3.3. Hereby the deviation due to the sagging of the fiber is approximately 0.8 cm (labeled  $x$  in figure 3.3) while the distance between the holding frames is 7.0 cm. Hence the distance  $y$  in figure 3.3 is 3.5 cm.

$$\Delta l_{\text{sagging}} = 2(\sqrt{x^2 + y^2} - y) \quad (3.2)$$

The length of the test section also increases if the fiber is placed slightly diagonal on the frame resulting in another term  $\Delta l_{\text{placement}} = 0.1$  cm. The combination of both terms  $\Delta l_{\text{sagging}} + \Delta l_{\text{placement}}$  results in an uncertainty within the length of the test section  $\Delta l$  of 0.2 cm and assuming a deviation in the fiber's thickness within  $0.5 \mu\text{m}$ , the estimations (3.3) and (3.4) are obtained through gaussian error propagation. It has to be noted that this error is asymmetric since the sagging can only lengthen the tested section, while the diameter of the fiber can differ in both directions.

$$\Delta R_+ = \frac{4\rho}{\pi} \sqrt{\left(\frac{\Delta l}{d^2}\right)^2 + \left(-\frac{2l\Delta d}{d^3}\right)^2} \approx 3.7\text{k}\Omega \quad (3.3)$$

### 3. Thermal behavior of carbon fibers

$$\Delta R_- = \left| -\frac{8\rho l \Delta d}{\pi d^3} \right| \approx 3.6 \text{ k}\Omega \quad (3.4)$$

The deviation caused by the difference of the fibers diameter dominates the one caused via the sagging.

The measurement error of the resistance  $\Delta R_{\text{mm}}$  was calculated by adding the last two digits with 0.5 % of the measured value in accordance to the multimeter's manual [Ben]. The obtained deviation is smaller than (3.3) indicating that the setup is prone to systematic error caused by the section's length and the fiber's thickness rather than statistical errors resulting from the method of measurement. This suggest to emphasize more on relative values within one fiber rather than focussing on the actual value.

The fiber could not be strained properly, so it is sagged and therefore the length of the measured section is increased. This results in a higher resistance compared to the calculated value, however every filament yields slightly lower values compared to the calculated resistance implying that the fiber's surface contains irregularities resulting in greater thickness and thereby smaller electrical resistance predominating the sagging effects.

The loss of the fiber labeled "2" indicates that the contact between the fiber and the copper plates is imperfect. The copper plates oxidate over time forming nonconductive copper oxide on the surface, which should result in an increase of the systematic error over time.

### 3.3. Thermal influences in vacuum and air

After verifying that a single filament is used, the fiber could be tested for the temperature dependance of its resistance. Before the measurement is performed, the voltage range 0 – 160 V is traversed to see whether a change in the fiber could be seen in air. It could qualitatively be observed that the fiber radiates heat. Increasing the voltage above 120 V, a slight glow of the fiber could be observed which increased in intensity at higher voltages. The same test is repeated in vacuum resulting in similar observations at lower voltages (figure 3.4). The fiber started to glow cherry-red, which indicates a temperature in the range of 700 – 800 °C. The Boudouard reaction<sup>2</sup> heavily favors the production of carbon monoxide within this temperature range indicating that the fiber reacted with the residual gas within the oven.

---

<sup>2</sup>  $C + CO_2 \rightarrow 2CO$ , named after Octave Leopold Boudouard

### 3. Thermal behavior of carbon fibers

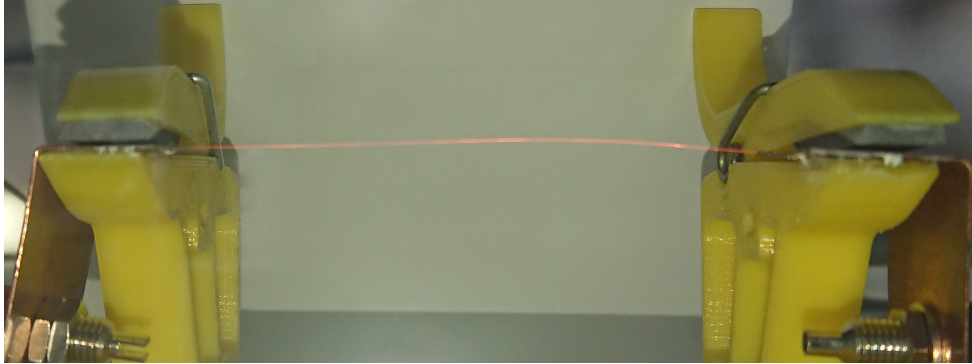


Figure 3.4.: Cherry-red glowing fiber in vacuum at around 90 V. In accordance to [AG.] this indicates a temperature of around 700 – 800 °C. At this temperature, the transition to carbon monoxide (CO) takes place.

It has to be noted, that its temperature can only be observed indirectly. A direct method can not be applied because on the one hand, a tactile method would distort the measurement too much due to the low thermal capacity of the fiber. On the other hand, the size of the fiber is too small for infrared temperature measurements.

Already one could see a correlation between the stability of the fiber and the induced power. The fibers started to rupture over time, setting a threshold of  $U_{\max, \text{air}} = 220 \text{ V}$  at which the longest lasting fiber broke. Once the threshold was verified by breaking more fibers at this voltage and it has been asserted that the corresponding threshold in vacuum is reached at lower voltages around  $U_{\max, \text{vac}} = 100 \text{ V}$ , the data acquisition was started. Therefor the circuit 3.1 is assembled. The data for current and voltage is manually read off the multimeters and recorded.

Meanwhile the heat emitted from the fiber could be observed using a infrared camera "FLIR i7". The camera is able to perform a rudimentary data aquisition by determining the temperature of the air around the fiber. The camera includes an algorithm that automatically finds the warmest point within the marked area and displays its temperature in the upper left corner.

### 3. Thermal behavior of carbon fibers

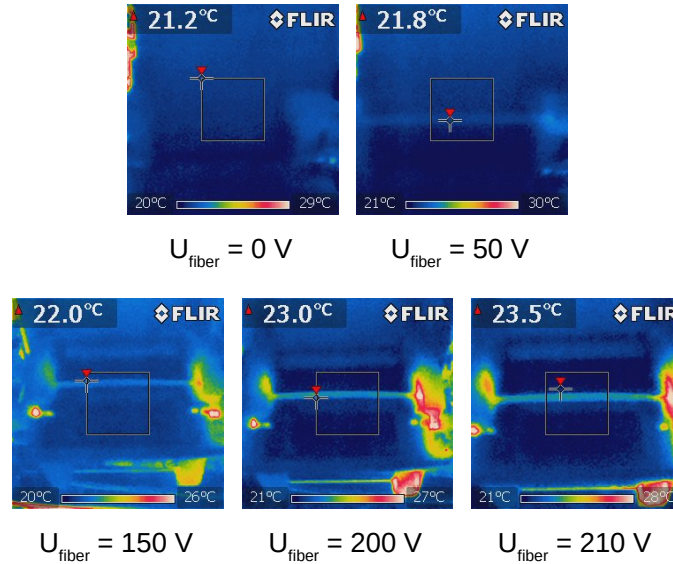


Figure 3.5.: Five pictures taken with an IR camera at different voltages

Within the marked area the maximum temperature is displayed in the top left corner. Increasing the voltage causes a visible hot air convection around the fiber. Also, the increasing surface temperature of the copper plates can be seen.

In the first picture ( $U_{\text{fiber}}=0$ ) of figure 3.5 the fiber can hardly be distinguished from the surroundings, but by applying voltage one can make out a thin area between the two clips of the holding frame. The temperature increases with the voltage.

First, the data for a measurement in air is recorded in the appendix A.1. During the same measurement, five pictures (figure 3.5) were taken with the infrared camera to visualize the change in the temperature around the fiber. The fiber started to glow around 180 V and broke at 215 V.

The next data was acquired in vacuum and in air with the same fiber. In figure 3.6 the data of all 3 measurements is displayed while in figure 3.7 only the data for fiber 2 is displayed in air and in vacuum since it is they are better comparable because both measurements are performed on the same fiber.

The relation in figure 3.6 is close to linear, implying that the fiber behaves as an ohmic resistance. Closer observation of the data shows that the current starts to flat out with rising voltages. In accordance to 1.8 this means that the resistance decreases with increasing temperature implying that the material did not exceed its threshold at around 500 °C at which the resistance starts to rise with increasing temperature.

This can be explained through the convection around the fiber as supported by figure

### 3. Thermal behavior of carbon fibers

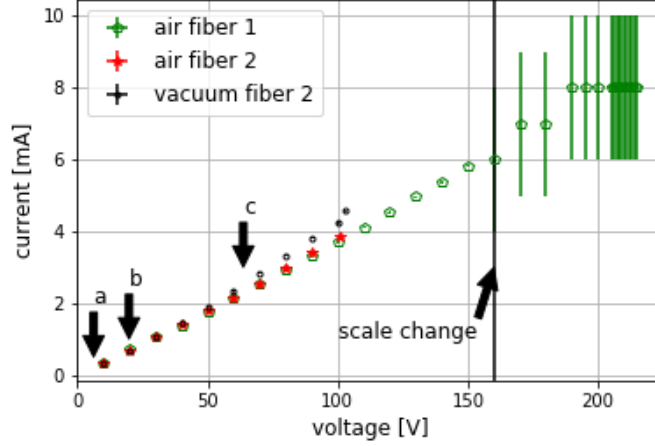


Figure 3.6.: Data obtained in air and vacuum

At 160 V the measuring scale of the multimeter is changed resulting in a loss of significant digits, however a general trend towards higher currents is observed within the data above 160 V. The fiber used during the recording of the green data broke at 215 V, the other fiber broke at 103 V while measuring in vacuum

The marked voltages correspond to the expected thermal stress in  $\overline{\text{PANDA}}$  at normal conditions (a, 6.2 V), 10 times normal (b, 19.8 V) and at beam center (c, 63.7 V). The corresponding currents are far below the critical value. The calculations for the expected voltages are described in chapter 3.4

3.6. With increasing voltages, the obtained values of the current rise more slowly in air indicating that the fiber must emit energy in form of heat. Figure 3.6 also shows the loss of significant digits through a change in the measuring scale of the multimeter from  $\mu\text{A}$  to A. This reduces the precision of the multimeter dramatically but was unavoidable due to the range of the  $\mu\text{A}$  scale.

The obtained data of electric current and voltage is converted into resistance and electric power using the equations (3.5) and (3.6).

$$R = \frac{U}{I} \quad (3.5)$$

$$P = U \cdot I = \frac{U^2}{R} \quad (3.6)$$

These calculations have been executed in tables A.3 and A.2. The uncertainty of the data resulted from Gaussian error propagation.

### 3. Thermal behavior of carbon fibers

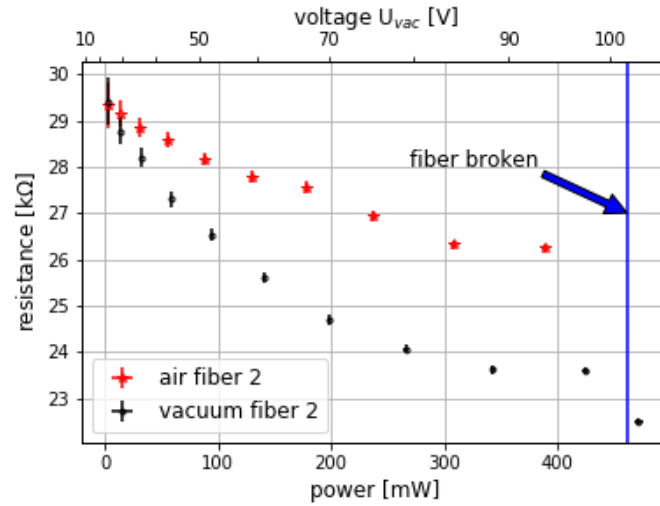


Figure 3.7.: Resistance over power obtained by increasing voltage and measuring current with the same fiber first in air and then in vacuum  
At the marked voltage the fiber started to rupture in vacuum leaving the last data point of the measurement in vacuum negligible.

Figure 3.7 displays the resulting data. The fiber ruptured at 98 V in vacuum as indicated by the blue line. The resistance development with increasing power is as expected. The decrease is steeper in vacuum since the convection is less dominant causing the fiber to heat up more quickly.

### 3.4. Simulation of thermal stress expected from $\overline{\text{PANDA}}$

The hypernuclear experiment at  $\overline{\text{PANDA}}$  is expected to run for 100 days. In the current design of the primary target, the carbon fiber must last at least 20 days inside the beam since five separate targets can be realized. To simulate the thermal stress caused by interference with the beam, the fiber is placed in the setup displayed in section 3.1 and a measurement of the current flowing through the fiber at constant voltage is conducted over time. During the measurement small changes in the voltage are observed, but only the mean voltage is recorded. The interval between each step is set to 10 seconds. Depending on the applied voltage, the time ranges from few minutes up to several days.

A thermal simulation of the primary target was conducted and displayed in the extract 1.6, resulting in the data presented in Table 3.2. This data is adjusted to fit the induced power over a 7 cm long section instead of 3 mm used in the simulation. This adjustment is performed by rule of proportion. The power per unit of length is constant allowing the rescaling via (3.7).

$$P_a = \frac{P_b}{b} \cdot a \quad (3.7)$$

If the fiber is able to withstand the maximum input at beam center, its stability in the experiment will be granted. Therefore these power inputs will be the base for further tests.

target material	P @ $R_{\text{exp}}$	P @ $10 \cdot R_{\text{exp}}$	P @ $R_{\text{max}}$
Dialead	1.3 mW	13.1 mW	165.7 mW
Sigrafil	1.3 mW	13.1 mW	135.4 mW

Table 3.2.: Recalculated power input for nine scenarios based on [Ble18]

In the original data, the power has been calculated for the expected rate of interaction  $R_{\text{exp}}$  as well as its ten times higher value and at beam center  $R_{\text{max}}$

The voltage corresponding to the calculated power can be obtained via (3.8).

$$U = \sqrt{PR} \quad (3.8)$$

U: applied voltage, P: power according to table 3.2, R: measured resistance

First, the voltage has been set to the maximum at around 100 V. The fiber started to glow after approximately 30 seconds and broke at 1:08 minutes.

The second test was conducted at 70 V, matching approximately half the power induced in the beam center. In this run the fiber lasted about 12 hours. Figure 3.8 shows the obtained data converted into resistance.

The data first shows a decrease in the resistance of the fiber which can be explained through the heating up of the fiber. Once the fiber reaches an equilibrium between its

### 3. Thermal behavior of carbon fibers

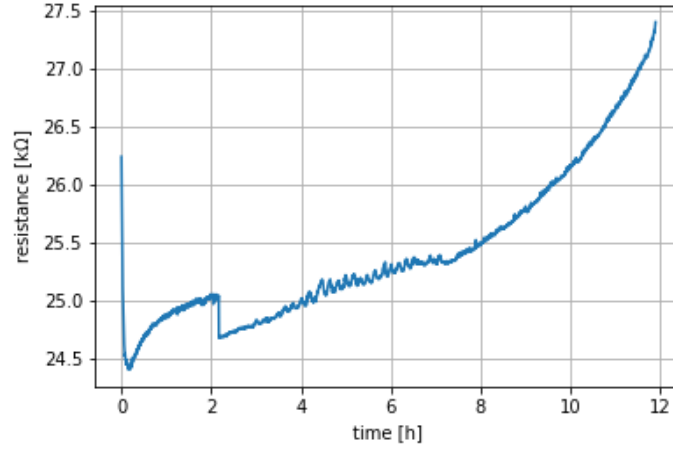


Figure 3.8.: resistance at 70 V over approximately twelve hours, at around 2 hours a sudden increase in the current is noted caused by a loose contact.

heating up due to the applied voltage and its radiation of heat, it starts to evaporate, causing the resistance to increase once again.

So far, the measurements showed that the fiber could withstand the thermal stress applied through the center beam only for a short period of time. The next measurement is intended to test the durability of the fiber at approximately 4 times the intended reaction rate at  $\bar{P}$ ANDA, translating to around 13 V according to equation (3.8) ( $P_{13V} = \frac{(13V)^2}{29.1k\Omega} = 5.8mW \approx 4P_{exp}$ ). This experiment lasted approximately 17 days after which it is terminated in order to conduct further testing. The fiber is still intact after this time. During the experiment, it was noted that the batteries of the multimeters wore down and had to be changed weekly. This discontinued the measurement for approximately 2 minutes and causes leaps in the measured data. Evaluating the obtained data displayed in figure 3.9 shows a consistent fluctuation in the recorded value and also some spontaneous drops and leaps not only when the batteries were changed. This is caused by a loose contact, which is also visible in the data displayed in 3.8 at approximately two hours. Ignoring the discontinuities, the resistance remains at the same level.

### 3. Thermal behavior of carbon fibers

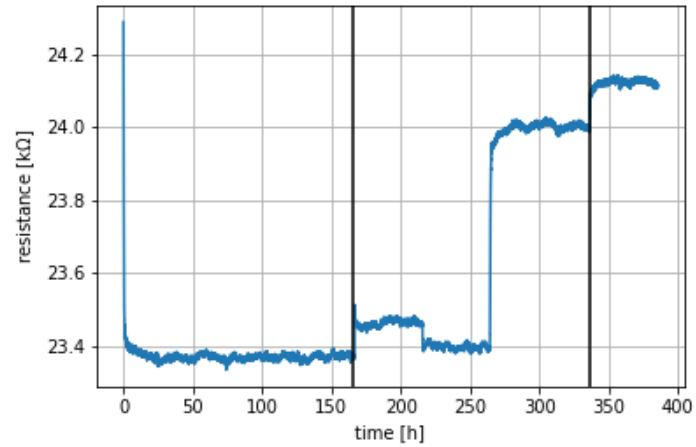


Figure 3.9.: data obtained at approximately 13 V. The lines indicate a short discontinuation in the measurement due to a change of battery in the multimeter

After adjusting the setup by brazing all contacts another test run was performed at approximately 57 V for 24 hours (figure 3.10). Once again the trends noted in the first measurement can be reproduced. Unfortunately the jitter and spontaneous drops still occurred indicating that the setup still has some flaws.

### 3. Thermal behavior of carbon fibers

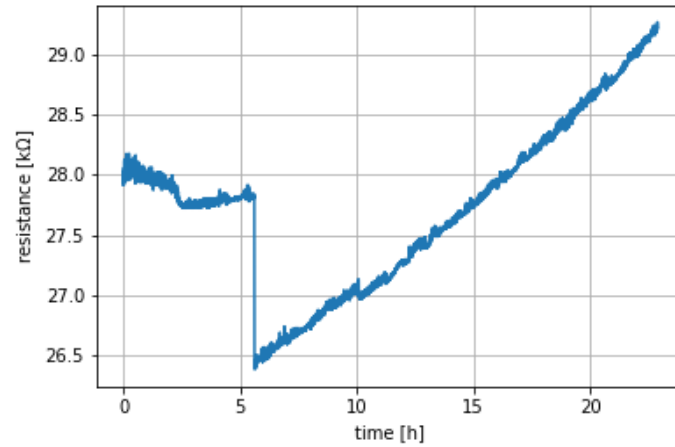


Figure 3.10.: Resistance at 57 V over approximately twenty-four hours, the data shows an overall jitter and a significant drop at around 5 h. This indicates that the setup can still be optimized.

In order to determine whether the flaw could be found within the contact between the copper plates and the filament the last measurement was repeated with the same fiber which is fixed at the copper plates via conductive silver varnish. The results from this run are displayed in figure 3.11.

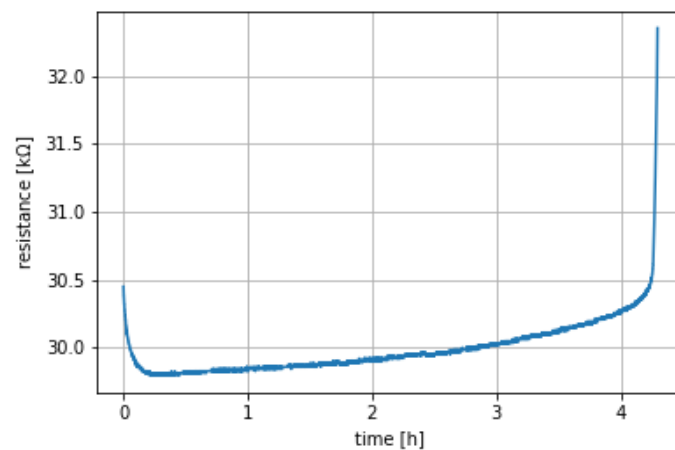


Figure 3.11.: Resistance at 57 V over approximately 4 hours, the same filament as in figure 3.10 is used but the contact is improved via conductive silver varnish

### *3. Thermal behavior of carbon fibers*

In this measurement no spontaneous drops were recorded and the jitter almost disappears implying that the contact has now been optimized. However the fiber only lasts for four hours before breaking. Its instability could be due to its earlier exposure and also due to mechanical stress applied through the varnish. The latter implies that the conductive silver varnish might not be suited to hold the fiber since it could be too unflexible to safely hold the heating, and therefore shrinking, fiber.

Compared to the last measurement, the preceding measurements can be revisited and analyzed as to where the contacts have been the worst.

Although the setup has some minor issues, the overall statement that the fiber is able to withstand prolonged exposure to thermal stress still holds true. The test at double the normal  $\bar{\text{P}}\text{ANDA}$  conditions shows no effect on the filament. At the maximum power expected from  $\bar{\text{P}}\text{ANDA}$ , the fiber is able to last long enough to allow a correction of its position but it is strained in that process reducing its life time.

## 4. Summary and outlook

To conclude this thesis its results will be summarized. First, a mechanical procedure to separate single filaments from a carbon fiber thread was looked into. Since the fiber Dialead was too brittle, no further studies could be performed on it. The separation of the Sigrafil carbon fiber thread is possible. Next, the glueing of the filament to a frame has been addressed. The general type of glue needed to fix the fiber onto its frame is best found in conductive carbon or a thermal adhesive that does not contain any silver ions.

The following experiments examined the thermal behavior of the fiber. While a direct heat measurement was not possible, the induction of current resulted in reliable data. It was found that the filament could withstand much higher power input both in air and vacuum than expected as thermal stress in  $\bar{\text{P}}\text{ANDA}$ . Also, a long-term measurement at approximately 4 times the power of the normal hypernuclear experiment could be performed over more than 16 days indicating the thermal stability of the fiber. It has been noted that the carbon filament can withstand stress similar to the expected thermal stress caused in the beam center at  $\bar{\text{P}}\text{ANDA}$  for just over one minute. This leaves enough time to register the change in the reaction rate and to adjust the fiber's position before the filament is lost.

The setup in the conducted experiments can still be optimized. Especially the connection between fiber and the copper plates should be reviewed. For the start, the additional conductive silver might suffice to improve the contact reducing the measurement uncertainty of the experiment. Regular cleaning of the copper plate should also increase the connectivity.

The carbon fiber appears to be an appropriate candidate as primary target at the hypernuclear  $\bar{\text{P}}\text{ANDA}$  experiment in terms of its durability under constant thermal stress. However further testing on the fiber should be conducted to see whether the filament can withstand the structural defects resulting from the interaction with the antiproton beam.

For a representative test of the irradiation properties of the filament, the thermal input must be equal. Assuming minimal ionizing particles, this means that the beam density must be equal. For proton accelerators it is hard to reach comparable densities without using a storage ring like COSY<sup>1</sup> at the Forschungszentrum Jülich and it is very unlikely to get multiple weeks of beam for this kind of tests.

For electrons more experiments might be available that can reach the required beam density, e.g. MAMI<sup>2</sup> in Mainz. One has to take into account that the effect of electrons on the displacement of atoms from the atomic lattice is reduced. Using the

---

<sup>1</sup>Cool Synchrotron

<sup>2</sup>Mainzer Microtron

#### *4. Summary and outlook*

information of [Spi12] 10 times more electrons are required to achieve the same effect in the filament. The factor even increases for lower beam momenta. Taking this factor into account the 20 days of PANDA beam need at least 200 days of MAMI beam for proper simulation. Again it is not likely that such a period of beam time is allocated to this test. Therefore real tests of the survivability have to wait on the HESR beam of PANDA.

# A. Appendix

## A.1. Production of carbon filaments via PAN

The fiber Sigrafil is produced from acrylonitrile, an organic compound with the formula  $\text{CH}_2\text{CHCN}$ . Through free-radical polymerization the compound polyacrylonitrile (PAN) is obtained. An oxidative cyclisation of PAN takes place at temperatures in

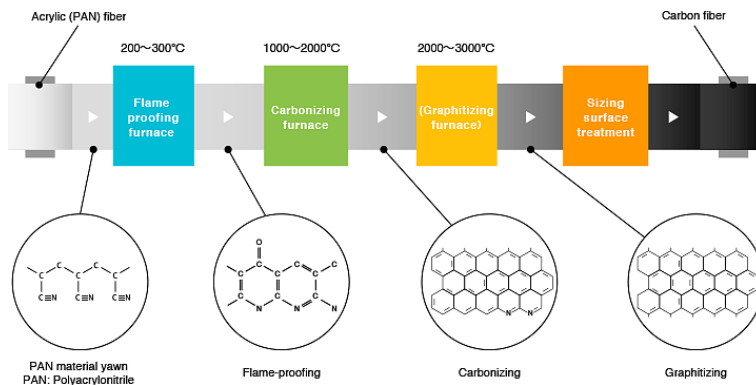


Figure A.1.: Conceptual synthesis of PAN based carbon fiber. This picture is taken from [TOR].

range of  $150\text{ }^\circ\text{C}$  to  $350\text{ }^\circ\text{C}$ , afterwards the fiber is once again treated with oxygen eliminating all excessive hydrogen through oxidation to water. Finally the fiber undergoes carbonization at  $1200 - 1500\text{ }^\circ\text{C}$  to suspend the nitrogen. At this stage the fiber is considered a high strength carbon fiber. The fiber "Sigrafil" is such a fiber.

If desired, the fiber can be graphitized. This results in a high module carbon fiber which shares most of the high strength carbon fibers physical traits but can not be stretched while also minimizing its mechanical resistance.

## A.2. Further figures and tables

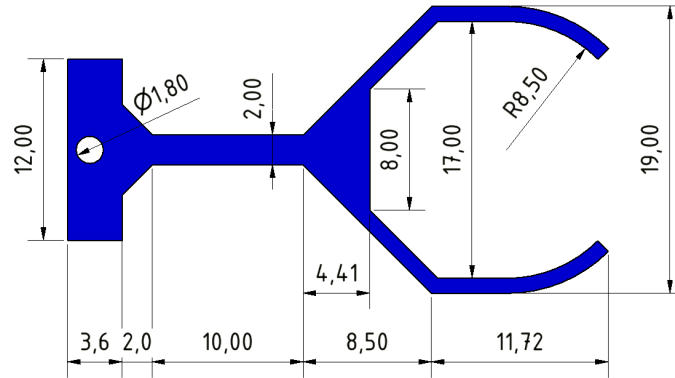


Figure A.2.: Conceptual design of the primary target frame as proposed in [Ble18].  
The unit of length is mm.

A. Appendix

U [V]	I [ $\mu$ A]	P [ $\mu$ W]	R [k $\Omega$ ]
10	336	3360	29.76
20	700	14000	28.57
30	1050	31500	28.57
40	1380	55200	28.99
50	1750	87500	28.57
60	2130	127800	28.17
70	2510	175700	27.89
80	2900	232000	27.59
90	3300	297000	27.27
100	3710	371000	26.95
110	4120	453200	26.70
120	4530	543600	26.49
130	4960	644800	26.21
140	5380	753200	26.02
150	5830	874500	25.73
160	6000	960000	26.67
170	7000	1190000	24.29
180	7000	1260000	25.71
190	8000	1520000	23.75
195	8000	1560000	24.38
200	8000	1600000	25.00
205	8000	1640000	25.63
206	8000	1648000	25.75
207	8000	1656000	25.88
208	8000	1664000	26.00
209	8000	1672000	26.13
210	8000	1680000	26.25
211	8000	1688000	26.38
212	8000	1696000	26.50
213	8000	1704000	26.63
214	8000	1712000	26.75
215	8000	1720000	26.88

Table A.1.: Table for measurement in air until the fiber 1 broke. The range of the multimeter has been changed at 160 V indicated by the double line.

A. Appendix

U [V]	I [ $\mu$ A]	P [ $\mu$ W]	R [k $\Omega$ ]
10	340	3400	29.41
20	695	13900	28.78
30	1064	31920	28.20
40	1465	58600	27.30
50	1885	94250	26.53
60	2343	140580	25.61
70	2835	198450	24.69
80	3325	266000	24.06
90	3810	342900	23.62
100	4240	424000	23.58
103	4580	471740	22.49

Table A.2.: Table for measurement in vacuum until fiber 2 broke

U [V]	I [ $\mu$ A]	P [ $\mu$ W]	R [k $\Omega$ ]
10	341	3410	29.33
20	686	13720	29.15
30	1040	31200	28.85
40	1400	56000	28.57
50	1775	88750	28.17
60	2160	129600	27.78
70	2540	177800	27.56
80	2970	237600	26.94
90	3420	307800	26.32
101	3850	388850	26.23

Table A.3.: Table for measurement in air with the same filament as in A.2

## Acknowledgment

Zu aller erst möchte ich mich bei Josef Pochodzalla, für die Möglichkeit eine Bachelorarbeit zu schreiben und die konstruktive Hilfe während des Verfassens der Arbeit, bedanken. Als zweites möchte ich Eva-Maria Kabuß dafür danken sich als zweiten Gutachter anzubieten.

Die Arbeitsgruppe hat mich vom ersten Moment an offen und hilfsbereit unterstützt. Für all die hilfreichen Diskussionen möchte ich mich herzlichst bei euch bedanken. In besonderer Weise geht mein Dank an Sebastian Bleser, der mich in die Gruppe aufgenommen hat und an Marcell Steinen, den ich auch wochenends noch mit meinen Fragen löchern durfte.

Zum Schluss möchte ich mich bei meinen Kommilitonen und Freunden bedanken die mich durch das Bachelorstudium hindurch begleitet haben und immer ein offenes Ohr hatten. Ebenso sei meinem Freund Marten und meiner Familie für ihre anhaltende Unterstützung, besonders auch meinen Eltern für die Finanzierung des Studiums, gedankt.

## B. Bibliography

- [AG.] Emil Vögelin AG.  
Glühfarben und temperatur von stahl.
- [Agi] *Agilent U1272A*.  
[http://www.produktinfo.conrad.com/datenblaetter/125000-149999/128025-da-01-en-AGILENT\\_U1272A\\_DMM\\_30000\\_COUNTS.pdf](http://www.produktinfo.conrad.com/datenblaetter/125000-149999/128025-da-01-en-AGILENT_U1272A_DMM_30000_COUNTS.pdf).
- [Arca] *Arctic MX-2*.  
[https://www.arctic.ac/de\\_de/mx-2.html](https://www.arctic.ac/de_de/mx-2.html).
- [Arcb] *Arctic Silver Thermal Adhesive*.  
[http://www.arcticsilver.com/arctic\\_silver\\_thermal\\_adhesive.htm](http://www.arcticsilver.com/arctic_silver_thermal_adhesive.htm).
- [Ben] *Benning MM10*.  
[http://www.produktinfo.conrad.com/datenblaetter/125000-149999/127912-an-01-ml-MM10\\_DIG\\_MULTIMETER\\_de\\_en\\_fr\\_nl\\_cs.pdf](http://www.produktinfo.conrad.com/datenblaetter/125000-149999/127912-an-01-ml-MM10_DIG_MULTIMETER_de_en_fr_nl_cs.pdf).
- [Ble18] S. Bleser.  
*The target system for the hypernuclear experiment at PANDA*.  
PhD thesis, Johannes-Gutenberg-University, Mainz, expected 2018.
- [Che] Mitsubishi Chemicals.  
web page, last accessed 10.02.2018.
- [Col05] PANDA Collaboration.  
Technical report for panda, 2005.
- [Diaa] *Pitch-based Carbon Fiber DIALEAD*.  
[https://www.m-chemical.co.jp/en/products/departments/mcc/cfcm/product/1201229\\_7502.html](https://www.m-chemical.co.jp/en/products/departments/mcc/cfcm/product/1201229_7502.html).
- [diab] *SC-CVD Diamond Properties*.  
[http://www.ddk.com/PDFs/SC-CVD\\_Diamond\\_Properties.pdf](http://www.ddk.com/PDFs/SC-CVD_Diamond_Properties.pdf)  
[http://www.ddk.com/PDFs/SC-CVD\\_Diamond\\_Properties.pdf](http://www.ddk.com/PDFs/SC-CVD_Diamond_Properties.pdf).
- [LFM62] É. N. Marmer L. F. Mal'tseva.  
Determination of the electrical properties of graphite at high temperatures.  
*Soviet Powder Metallurgy and Metal Ceramics*, 1, 1962.  
Studies concerning thermal behavior of carbon.
- [Pat] *Pattex Ultra Gel*.  
[http://mymsds.henkel.com/mymsds/0001.1359687.3610.de.MSDS\\_UT\\_DE.DE.pdf](http://mymsds.henkel.com/mymsds/0001.1359687.3610.de.MSDS_UT_DE.DE.pdf).

## B. Bibliography

- [Roj16] M. M. Rojo.  
Design, construction and test of the primary target system for panda.  
Master's thesis, Johannes-Gutenberg-University, Mainz, January 2016.
- [Sig] *SIGRAFIL Continuous Carbon Fiber Tow*.  
[http://www.sglgroup.com/cms/\\_common/downloads/products/product-groups/cf/carbon-fiber-continuous-tow/SIGRAFIL\\_Continuous\\_Carbon\\_Fiber\\_Tow\\_e.pdf](http://www.sglgroup.com/cms/_common/downloads/products/product-groups/cf/carbon-fiber-continuous-tow/SIGRAFIL_Continuous_Carbon_Fiber_Tow_e.pdf).
- [So16] B. Singh and other.  
Study of doubly strange systems using stored antiprotons.  
*Nuclear Physics A*, 954:323 – 340, 2016.  
Recent Progress in Strangeness and Charm Hadronic and Nuclear Physics.
- [Spi12] Helmuth Spieler.  
Solid state detectors – vii. radiation effects, uspas-msu course.  
[http://www-physics.lbl.gov/~spieler/USPAS-MSU\\_2012/pdf/VII\\_Radiation\\_Effects.pdf](http://www-physics.lbl.gov/~spieler/USPAS-MSU_2012/pdf/VII_Radiation_Effects.pdf), june 2012.
- [Tar] *RS 186-3593*.  
<http://docs-europe.electrocomponents.com/webdocs/001d/0900766b8001d974.pdf>.
- [TOR] TORAYCA.  
web page, last accessed 11.02.2018.
- [Uhu] *Uhu All-Purpose Adhesive*.  
<http://www.uhu.com/print/de/produkte/alleskleber/detail/uhu-vielzweckkleberflinke-flascheohne-loesungsmittel.html?cHash=246759b678026911af524f238480f4c1&step=346.5>.

## C. List of Figures

1.1.	FAIR's conceptual setup . . . . .	1
1.2.	overview of $\overline{\text{P}}\text{ANDA}$ . . . . .	2
1.3.	hypernuclei production . . . . .	3
1.4.	primary target . . . . .	4
1.5.	Extract: suitability . . . . .	5
1.6.	Extract: Table from heat simulation . . . . .	5
1.7.	Extract: thermal expectations . . . . .	6
1.8.	Extract: thermal behaviour . . . . .	7
2.1.	fiber thread . . . . .	9
2.2.	metal tool with frame . . . . .	10
2.3.	frame with filament . . . . .	11
3.1.	circuit . . . . .	14
3.2.	holding device . . . . .	15
3.3.	length approximation . . . . .	17
3.4.	glowing fiber . . . . .	19
3.5.	infrared pictures . . . . .	20
3.6.	data: I vs. U . . . . .	21
3.7.	data: R vs. P . . . . .	22
3.8.	data: R vs. t (70 V) . . . . .	24
3.9.	data: R vs. t (13 V) . . . . .	25
3.10.	data: R vs. t (57 V) . . . . .	26
3.11.	data: R vs. t (57 V, optimized) . . . . .	26
A.1.	conceptual synthesis . . . . .	30
A.2.	frame . . . . .	31

## D. List of Tables

1.1. comparison . . . . .	6
3.1. resistance . . . . .	16
3.2. recalculated power . . . . .	23
A.1. data: air, fiber 1 . . . . .	32
A.2. data: vacuum, fiber 2 . . . . .	33
A.3. data: air, fiber 2 . . . . .	33